



Coring tools have an effect on lithification and physical properties of marine carbonate sediments

David De Vleeschouwer¹, Theresa Nohl^{1,2}, Christian Schulbert³, Or M. Bialik¹, and Gerald Auer⁴

¹Institute of Geology and Paleontology, University of Münster, Corrensstr. 24, 48149 Münster, Germany

²Institute of Palaeontology, University of Vienna, Josef-Holaubek-Platz 2 (UZA II), 1090 Vienna, Austria

³Geozentrum Nordbayern, Section Palaeontology, Friedrich-Alexander University Erlangen–Nürnberg (FAU),
Loewenichstr. 28, 91054 Erlangen, Germany

⁴University of Graz, Department of Earth Sciences, NAWI Graz Geocenter,
Heinrichstraße 26, 8010 Graz, Austria

Correspondence: David De Vleeschouwer (ddevlees@uni-muenster.de)

Received: 20 June 2023 – Revised: 9 August 2023 – Accepted: 11 August 2023 – Published: 26 October 2023

Abstract. The International Ocean Discovery Program (IODP) *JOIDES Resolution* Science Operator typically uses an advanced piston corer (APC) in soft ooze and sediments and an extended core barrel (XCB) in firm sediments. The coring tool exchange typically occurs around the same depth in adjacent holes of the same site. However, during IODP Expedition 356, the coring tool switch occurred at different depths: IODP Sites U1463 and U1464 are marked by a stratigraphic interval (> 25 m thick) that was XCB cored in one hole and APC cored in other holes. Shipboard scientists remarked that APC-cored sediments were unlithified or partially lithified, while XCB-cored sediments were fully lithified. This difference in sedimentological description of the same formation seems to be an effect of coring technique. To provide further insight, we assessed the physical properties (bulk density, porosity, and P-wave velocity), downhole wireline logging data, scanning electron microscope (SEM) images, and micro-computed tomography (μ CT) scans of those intervals.

We find systematic differences between the different coring techniques. XCB cores are characterized by systematically lower bulk density, higher porosity, and higher P-wave velocity than APC cores. Downhole logging data suggest that the original P-wave velocity of the formation is better preserved in XCB cores, despite the typical “biscuit-and-gravy” core disturbance (i.e. well-preserved core fragments surrounded by squelched core material). In conjunction with SEM and μ CT images, we conclude that the APC tool destroyed early lithification by breaking cements between individual grains. Moreover, μ CT images reveal denser packing and smaller pore volumes in the APC cores. These sedimentary changes likely occur when the APC pressure wave passes through the sediment. The destruction of grain-to-grain cements provides an explanation for the significantly lower P-wave velocities in APC cores. Interestingly, the gravy sections in XCB drilled cores mimic the destruction of early lithification and reduction of pore volume. We conclude that APC remains the tool of choice for recovering soft sediments, especially for paleoclimate purposes. However, for the study of lithification, XCB biscuits provide a more representative image of the formation. For the study of early diagenesis, further studies are required to ascertain the preservation of key sedimentary features using existing and new drilling tools.

1 Introduction

Lithification is the process by which loose sediment is transformed into solid rock. This transformation can involve biochemical, physicochemical, and mechanical processes at different stages of burial, from cementation and dissolution-precipitation at the seafloor to pressure-/temperature-induced alteration in several hundreds of metres of depth (Shinn, 1969; Garrison and Kennedy, 1977; Herbert, 1993; Buryakovskiy et al., 2012; Sample et al., 2017; Ge et al., 2020; Sulpis et al., 2022).

In the case of carbonate sediment, the main lithification pathway is cementation, in which minerals such as calcite, aragonite, or dolomite precipitate from interstitial water and fill the spaces between carbonate and detrital grains. Thereby, a solid matrix originates, which binds together the grains. Cementation can manifest in different forms: (1) the presence of cements that provide insights into the depositional or diagenetic environment (Friedman, 1964; Bathurst, 1972, 1974, 1980; Flügel, 1982); (2) the transformation of mud into micrite during early diagenesis, a process known as micritization (Folk et al., 1965; Munnecke, 1997; Munnecke et al., 2023); (3) late diagenetic transformations such as pressure dissolution (Moore and Wade, 2013); (4) dolomitization, during which dolomite replaces the original mineral composition (Budd, 1997; McKenzie and Vasconcelos, 2009; Mavromatis et al., 2014; Reuning et al., 2022); and (5) the diagenetic transformation of any of the four cases mentioned (Harris et al., 1985). Lithification and cementation modify the physical properties of the sediment, including porosity, density, and P-wave velocity (Fabricius, 2003). However, the precise mechanisms behind these transformations remain a topic of ongoing debate. However, it is clear that, when sediments undergo the process of cementation and mineral grains bind together, and when compaction is caused by the pressure of overlying sediments, loose sediments gradually transform into a resilient and lithified carbonate rock.

Identifying and separating the processes that drive lithification is crucial to infer original paleo-environmental information. Doing so becomes exceedingly complicated as several aspects of lithifying carbonate sediments are still not understood. Especially the early diagenetic transformation of soft sediments into solid rock remains enigmatic (Reid et al., 2000; Nohl et al., 2021; Tagliavento et al., 2021; Reuning et al., 2022; Munnecke et al., 2023). What can be inferred is that the microbial decay of organic matter causes variable geochemical gradients impacting porewater alkalinity and pH, which leads to the dissolution of aragonite and a reprecipitation of CaCO_3 as calcite cement (Froelich et al., 1979; Berner, 1980; Munnecke and Samtleben, 1996; Soetaert et al., 2007; Wurgaft et al., 2019; Reuning et al., 2022). However, the exact processes leading to dissolution and precipitation of CaCO_3 , the exact depth within the sediment column, and the source of both calcium and carbonate in interstitial waters, remain largely unconstrained and thus under

debate. The existence of this knowledge gap holds significant implications, as the dissolution of substantial portions of carbonate sediment, such as aragonite in modern sediments, has the potential to be transported back into the seawater. Furthermore, lithological alternations, such as between limestone and marl, are often used for cyclostratigraphic purposes, introducing interpretations in terms of past climate change and new chronostratigraphic information (Sinnesael et al., 2019). However, the robust identification of lithological cyclicity and its attribution to Milankovic forcing requires insights into the lithification process and the early diagenetic history of sediments in different depositional environments. Such insights start with correctly observing and pinpointing the transition of unlithified into lithified sediment in modern systems. Moreover, the degree to which sediment is lithified has further implications for reconstructing faunal composition and abundance. Indeed, several processes involved in lithification act as a taphonomic filter (Hendy, 2011; Nawrot, 2012; Nohl et al., 2019).

Scientific drilling within the International Ocean Discovery Program (IODP) framework provides an opportunity to identify and analyse the transition from unconsolidated to lithified sediments beneath the current seafloor. Curiously though, IODP Expedition 356 shipboard scientists noted that the lithification description of a particular formation was dependent on the coring technique employed (Gallagher et al., 2017a). On this expedition, the RV *JOIDES Resolution* deployed the four standard wireline coring tools: the advanced piston corer (APC), the half-length advanced piston corer (HLAPC), the extended core barrel (XCB), and the rotary core barrel (RCB). In sedimentary layers of alternating hardness, like on Expedition 356, a typical coring strategy is to change back and forth between the use of the APC, the HLAPC, and the XCB to best capture the full stratigraphy. This coring strategy had the consequence that at multiple sites, the same formation was cored by the XCB in one hole and by the (HL)APC in other holes. Thereby, the same stratigraphic interval, cored by different coring techniques, yielded differently lithified sediments. Typically, the APC-cored sediments in one hole were described as unlithified or partially lithified, while XCB-cored sediments in the other hole were assessed to be fully lithified. In this paper, we evaluate the effect of coring tools on lithification and physical properties of marine sediments in order to obtain new insights into the transition from soft sediment to lithified rock in an IODP context, as well as to report a potential bias introduced by the choice of coring tool.

2 Materials and methods

2.1 IODP sites at which the same formation was recovered using different coring tools

2.1.1 Site U1463

Site U1463 (141 m water depth; Fig. 1) is situated on a flat outer ramp, with a seabed that consists of poorly sorted carbonate-rich sediment (bioclastic gravel, sand, and mud). Site U1463 is subdivided into five lithostratigraphic units: from top to bottom, Site U1463 consists of unlithified wackestone and mudstone with abundant peloids (Unit I); alternating unlithified wackestone, packstone, and mudstone intervals (Unit II); well-sorted homogeneous mudstone containing fine sand-sized grains (Unit III, both described as lithified and unlithified); lithified grainstone with abundant macrofossils (Unit IV); and lithified dolostone with sand-sized pyrite and glauconite grains (Unit V). Unit III contains the stratigraphic layers that were cored with different coring tools: this interval of interest extends between 280–400 m core depth below sea floor (CSF-A). It was cored with the XCB in Hole U1463B (U1463B 34X–46X), with the HLAPC in Hole U1463C (U1463C 33F–61F) and with both the APC and the HLAPC in Hole U1463D (U1463D 32H–47F). The different holes of a single site can be considered as sampling the same stratigraphic interval, as the research vessel was only offset by 20 m between the different holes. Potential differences in lithification and physical properties of the same formation between the different holes can therefore only be explained by the coring tools used.

2.1.2 Site U1464

Site U1464 is also situated within an outer ramp setting (270 m water depth), about 100 km northeast of Site U1463 and 50 km southeast of the Rowley Shoals. The site is located adjacent and shoreward to a drowned “fossil” reef/shoal (~ 5 km; Ryan et al., 2009). Site U1464 is divided into five lithostratigraphic units: from top to bottom, Site U1464 consists of unlithified sediments with peloids in varying abundances (Unit I), unlithified homogeneous wackestone including a packstone interval (Unit II), unlithified homogeneous mudstone (Unit III), dolomitic limestone and dolostone (Unit IV, described as lithified and unlithified, and V, described as lithified). The stratigraphic layers that were cored with different coring tools belong to the bottom of Unit III and the topmost part of Unit IV: the interval of interest extends between 285–315 m CSF-A. It was cored with the APC and the HLAPC in Hole U1464B (U1464B 33H–35F), with the RCB in Hole U1464C (U1464C 2R–3R) and with the XCB in Hole U1464D (U1464D 33X–34X). Similar to Site U1463, the vessel was offset by 20 m for coring the different holes of Site U1464.

2.1.3 Site U1482

Site U1482 (IODP Expedition 363) is a further site offshore northwest Australia that has a significant stratigraphic interval cored by several coring tools. Between 340 and 380 m CSF-A, Hole U1482A and U1482B were cored with the HLAPC (U1482A 38F–45F and U1482B 41F–45F), while U1482C was cored with the XCB (U1482C 39X–42X). Nevertheless, this site is not discussed further in this paper because discrete bulk density, porosity, and P-wave velocity measurements of these sediments were only measured in U1482A in the interval of interest, and the shipboard sedimentologists did not explicitly report the degree of lithification. These two factors result in the available shipboard data not allowing for a detailed comparison of sediment properties between different coring tools. The physical property data obtained with the whole-round multisensor logger (WRMSL) do not provide a suitable alternative because of the difference in diameter between the APC and XCB cores. The Expedition 363 shipboard scientists attempted to correct for this effect by applying an XCB correction factor, but their attempt was unsatisfactory as it introduced significant offsets between whole-round and discrete measurements further downcore (Rosenthal et al., 2018).

2.2 Shipboard discrete moisture and density and P-wave velocity measurements

We only consider shipboard physical property measurements carried out on discrete samples (bulk density and porosity) and directly on the split-core surface (P-wave). Hence, we do not consider physical property measurements carried out on whole-round sections because their results are strongly affected by the extent to which the core liner is filled with sediment.

Discrete samples were collected shipboard from the working halves to determine wet and dry bulk density, grain density, water content, and porosity. A detailed description of the analytic procedure can be found in Gallagher et al. (2017b), who followed the guidelines provided in Blum (1997). Here, we provide a short summary of the applied methods. Sediment samples were placed in Wheaton glass or plastic vials before wet and dry sediment weighing. The weights of wet and dry sample masses (M_{wet} and M_{dry}) were determined to a precision of 0.005 g using two Mettler Toledo electronic balances, with one acting as a reference. A standard weight of similar value to the sample was placed on the reference balance to increase accuracy. A computer averaging system was used to compensate for the ship’s motion. The default setting of the balances is 300 measurements (taking ~ 1.5 min). Dry sample volume (V_{dry}) was determined using a hexapycnometer system of a six-celled custom-configured Micromeritics AccuPyc 1330TC helium-displacement pycnometer. The precision of each cell is 1 % of the full-scale volume. Volume measurement was preceded by three purges of the sample

chamber with helium warmed to $\sim 28^\circ\text{C}$. Three measurement cycles were run for each sample. A reference volume (set of two calibration spheres) was placed sequentially in one of the chambers to check for instrument drift and systematic error. The volumes occupied by the numbered vials were calculated before the cruise by multiplying each vial's weight by the average density of the vial glass. Dry mass and volume were measured after samples were heated in an oven at $105^\circ\text{C} \pm 5^\circ\text{C}$ for 24 h and allowed to cool in a desiccator. The mass of the evaporated water (M_{water}) and salt (M_{salt}) in the sample are given by

$$M_{\text{water}} = M_{\text{wet}} - M_{\text{dry}}$$

$$M_{\text{salt}} = M_{\text{water}} \left[\frac{s}{1-s} \right],$$

where s is the assumed saltwater salinity (0.035) corresponding to the pore water density (ρ_{pw}) of 1.024 g cm^{-3} and a salt density (ρ_{salt}) of 2.22 g cm^{-3} . The corrected mass of pore water excluding salt (M_{pw}), the volume of pore water (V_{pw}), the volume of salt (V_{salt}), and wet volume (V_{wet}) are

$$M_{\text{pw}} = \frac{M_{\text{water}}}{1-s}$$

$$V_{\text{pw}} = \frac{M_{\text{pw}}}{\rho_{\text{pw}}}$$

$$V_{\text{salt}} = \frac{M_{\text{salt}}}{\rho_{\text{salt}}}$$

$$V_{\text{wet}} = V_{\text{dry}} - V_{\text{salt}} + V_{\text{pw}}.$$

Wet bulk density (ρ_{wet}) and porosity (ϕ) are calculated as

$$\rho_{\text{wet}} = \frac{M_{\text{wet}}}{V_{\text{wet}}}$$

$$\phi = \frac{V_{\text{pw}}}{V_{\text{wet}}}.$$

Moisture and density measurements during Expedition 356 were calculated with the MADMax shipboard programme, set with the "Method C" calculation process.

2.3 Downhole logging

At Site U1463, downhole measurements were conducted in Hole U1463B. The porosity and bulk density of the formations were measured with the Accelerator Porosity Sonde (APS) and the Hostile Environment Litho-Density Sonde (HLDS), respectively. Both tools were part of the triple combo tool string that was run between 452 m wireline log-matched depth below seafloor (WMSF) and the seafloor. The results were judged to be of very good quality, based on the systematic variation in the logs, the standoff distance between the tool and the borehole wall, and the consistency with the discrete moisture and density measurements on

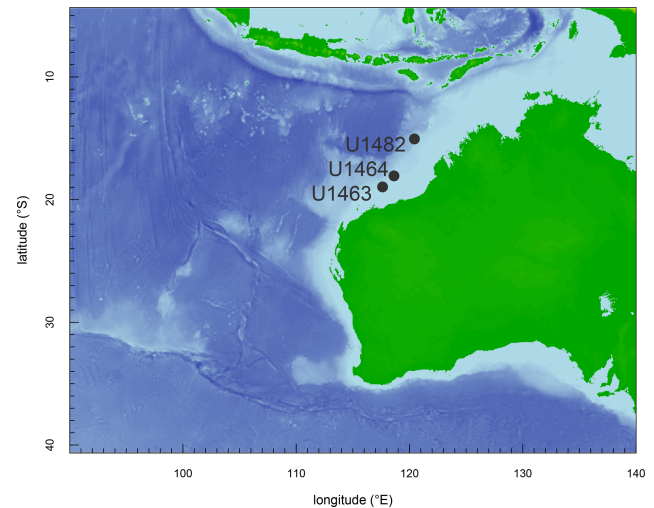


Figure 1. Map of the studied sites on the North West Shelf of Australia.

cores (Gallagher et al., 2017c). Sonic P-wave velocities along the borehole wall were determined by the dipole sonic imager (DSI) mounted on the Formation Micro Scanner (FMS)-sonic tool string. At Site U1463, the FMS-sonic string was deployed between 444–122 m WMSF. The downhole sonic velocities are considered to be of good quality because the FMS made full contact with the borehole wall, and the FMS resistivity images are generally of good quality (Gallagher et al., 2017c). At Site U1464, the wireline tool became stuck in the hole below the interval of interest on the first pass up with the triple combo tool string. Unfortunately, the HLDS and APS were turned off during the down pass, and downhole logging with the FMS-sonic was not attempted following the recovery of the triple combo. These circumstances imply that Site U1464 does not have wireline logging data that can be used to groundtruth bulk density, porosity, and P-wave velocity data from cores.

The HLDS contains a radioactive ^{137}Cs gamma ray source (622 keV) and far and near gamma ray detectors mounted on a shielded skid, which is pressed against the borehole wall by a hydraulically activated decentralizing arm. Gamma rays emitted by the source undergo Compton scattering, in which gamma rays are scattered by electrons in the formation. The number of scattered gamma rays that reach the detectors is proportional to the density of electrons in the formation, which is, in turn, related to bulk density.

The APS includes a Minitron neutron generator that produces fast (14.4 MeV) neutrons and five detectors positioned at different distances from the Minitron. The tool counts neutrons that arrive at the detectors after being scattered and slowed by collisions with atomic nuclei in the formation. The highest energy loss occurs when neutrons collide with hydrogen nuclei, which have practically the same mass as the neutron (the neutrons bounce off of heavier elements without

losing much energy). In low-porosity formations, neutrons can travel farther before being captured, and the count rates increase at the detector. However, because hydrogen bound in minerals such as clays or hydrocarbons also contributes to the measurement, the raw porosity value is often overestimated.

The DSI measures the transit times between sonic transmitters and an array of eight receivers. It combines replicate measurements, thus providing a direct measurement of sound velocity through formations. Along with the monopole transmitters found on most sonic tools, the DSI also has two crossed-dipole transmitters that allow the measurement of shear wave velocity in addition to compressional wave velocity. Dipole measurements are necessary to measure shear velocities in slow formations, with shear velocity less than the velocity of sound in the borehole fluid. Such slow formations are typically encountered in deep-ocean drilling.

2.4 Micro-computed tomography (CT) scans

Six micro-CT scans were performed with the General Electric Phoenix V|tome| × S240 of the Palaeontology section of the Geozentrum Nordbayern at the University of Erlangen–Nürnberg, Germany. The micro-CT was equipped with the Phoenix 180NF x-ray source with a high-energy target (tungsten on diamond window) and the Phoenix DXR 250RT detector at 200 μm pixel size and 1.000 × 1.000 pixels. Scanning was done with 100 kV and 100 μA at a resolution of 10 μm in a collimated cone beam and a 0.1 mm copper filter. Raw data were reconstructed with Phoenix Datos| × software using a GPU-supported Feldkamp algorithm based on filtered backprojection. CT data post-processing was performed with the ORS Dragonfly software version 2023.2 on a Windows 10 workstation. For noise reduction of the reconstructed data sets within Dragonfly, a Gaussian filter (3-D mode, kernel-size 3) was used. From all data sets, a central cube-shaped volume of 4 mm edge length was selected as a sample volume for the pore analysis. To detect the pores from the material of the samples, a threshold was defined to distinguish pore volume from material volume. To eliminate noise and artefacts, all pores smaller than 27 voxels were excluded from the analysis. For visualization, the pore spaces were rendered in 3-D with a colour scheme according to the respective volume (number of voxels) of the pores.

2.5 Scanning electron microscope (SEM)

Six samples were imaged using a Zeiss Gemini DSM982 field-emission scanning electron microscope at the University of Graz, Department of Earth Sciences. For each sample, several fracture pieces were mounted on a standard SEM stub using conductive graphite tape before being coated with a carbon / platinum coating using a Leica EM ACE600 sputter coater. We applied a combination of external and in-lens secondary electron (SE) detectors for high-resolution imaging

(up to 100 000×). External and in-lens SE signals were combined using the DISS5 imaging software (point electronic GmbH) and dynamically adapted to maximize image contrast for individual grains and early diagenetic features for each image.

3 Results

This paper is motivated by the first remarkable observation that the degree of lithification reported for exactly the same stratigraphic interval by the shipboard sedimentologists varies depending on the coring technique used (as shown for U1463 and U1464 in Figs. 2 and 3, respectively). At Hole U1463B, the sediment became increasingly stiff at ~285 m CSF-A, which is where the drillers switched from HLAPC to XCB coring. In the next hole, Hole U1463C, the strategy was to use HLAPC cores until refusal, which happened at ~292 m CSF-A. The XCB-obtained U1463B interval displays a type of core disturbance referred to as “biscuits and gravy”. The XCB coring tool is designed such that the inner core liner does not rotate together with the drilling bit. Thereby the transfer of rotary torque from the cutting shoe to the cored formation is reduced yet not entirely eliminated (JOIDES Resolution Science Operator, 2014). This torque-transfer phenomenon entails the fragmentation of the cored material into distinct chunks, known as “biscuits”. The rotary motion of the core barrel in XCB drilling causes the biscuit fragments to rub against each other, resulting in the formation of ground sediment. The slurry created by mixing the ground sediment with drilling fluid and seawater is what generates the “gravy”. Gravy is typically observed in the core around and between the biscuits. Since biscuits provide a more accurate representation of the cored lithology, they are chosen for shipboard discrete physical property measurements (as shown in Figs. 2 and 3) and used for the sedimentological core description. Thereby, it is remarkable that the U1463B XCB biscuits between 330–400 m CSF-A are described as “lithified”, whereas the HLAPC cores from exactly the same stratigraphic interval in U1463C were reported to be only partially lithified (Fig. 2). The same contrasting pattern can be observed at Site U1464. There, XCB cores in Hole U1464D between 307–317 m CSF-A are described as lithified, contrary to the (HL)APC cores in the same stratigraphic interval, which were unlithified (Fig. 3). This significant variation in sediment description is not due to changes between night and day shifts but rather reflects a systematic difference in the external appearance of sediment cores from the same stratigraphic interval, depending on the coring tool used.

3.1 Physical properties

At Site U1463, the physical properties (bulk density, porosity, P-wave velocity) from discrete measurements show systematic differences between holes. The XCB cores from Hole

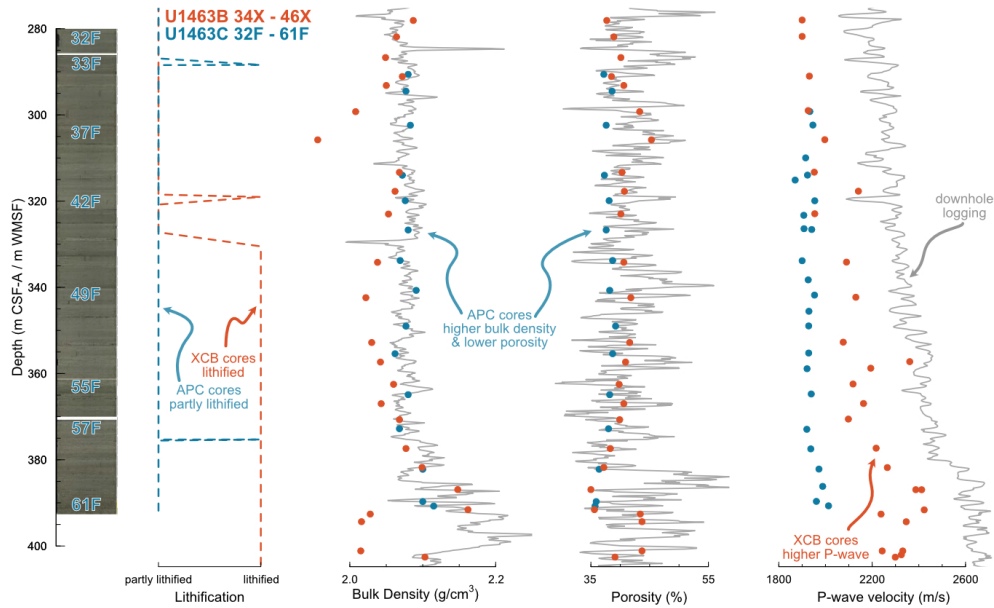


Figure 2. Lithification, bulk density, porosity, and P-wave velocity data measured at Site U1463. Orange data originate from XCB cores (Hole U1463B), blue data refer to HLAPC cores (Hole U1463C), and grey data reflect wireline logging data. Note that biscuits were selected for discrete physical property measurements on XCB cores.

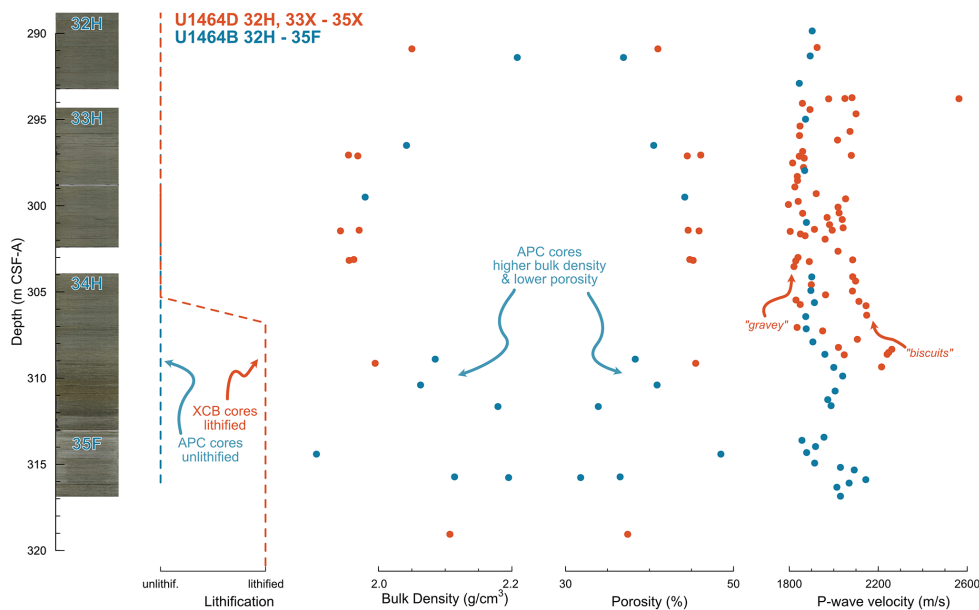


Figure 3. Lithification, bulk density, porosity, and P-wave velocity data measured at Site U1464. Orange data originate from XCB cores (Hole U1463D), blue data refers to (HL)APC cores (Hole U1464B). Note that biscuits were selected for discrete physical property measurements on XCB cores. Discrete P-wave velocity measurements constitute an exception as both biscuits and gravey were measured from XCB cores, with a bimodal distribution in the obtained velocities.

U1463B are characterized by systematically lower bulk density, higher porosity, and higher P-wave velocities (orange data in Fig. 2) compared to the HLAPC cores from Hole U1463C (blue data in Fig. 2). When compared to the in situ downhole logging wireline data, it seems that the bulk density data from the HLAPC cores are in closer agreement with

the wireline data. However, the offset in bulk density between HLAPC and XCB cores is often smaller than 0.05 g cm^{-3} , which is of the same order as the variability in the wireline data. For porosity, the offset between coring techniques is only a few percent. The HLAPC-XCB porosity offset is thus dwarfed by the large variability that marks the wire-

line porosity data. We note that the wireline porosity data often reflect an overestimate of the true porosity of the formation (see “Materials and methods”). This is especially the case for clay-rich formations like the studied interval. However, despite this consideration, it is not possible to determine whether HLAPC or XCB porosity data align more closely with the downhole logging data. On the other hand, the P-wave velocity data show a very clear picture, with the XCB cores approaching the downhole logging data more closely than the HLAPC data. This observation is independent of a possible mismatch between depth scales. In this respect, we note that core-based measurements are reported along the CSF-A depth scale, whereas the wireline data use the WMSF depth scale. The relation between both depth scales was determined by the correlation of distinctive features in core-based and wireline NGR (natural gamma radiation; Christensen et al., 2017; Gallagher et al., 2017c) and amounts between 3 and 6 m in the studied interval.

At Site U1464, downhole wireline logging attempts with the HLDS, APS, and DSI were unsuccessful at Site U1464, preventing any core–log comparisons. Nevertheless, one can observe similar patterns in terms of physical properties at Site U1464 compared to Site U1463. The XCB cores from Hole U1464D generally display lower bulk density and higher porosity (orange data in Fig. 3) compared to the (HL)APC cores from Hole U1464B (blue data in Fig. 3). Furthermore, and again similar to Site U1463, the highest P-wave velocities at U1464 come from XCB cores. However, the pattern becomes more nuanced, with P-wave velocities obtained from XCB cores from Hole U1464D falling into two distinct velocity end members. Low XCB P-wave velocities correspond to fine-grained pseudo-laminar material (gravy) that is considered to be drilling slurry, whereas the higher velocities are from hard, coarser-grained semi-lithified and less disturbed portions of the core (biscuits). The low-velocity end member of the XCB cores neatly corresponds to the velocities observed in APC cores from Hole U1464B. The high-velocity end member of the XCB cores is offset by $\sim 150 \text{ m s}^{-1}$.

The effect of the biscuit-and-gravy core disturbance is not limited to P-wave velocity. Bulk density data obtained by the whole-round logger for XCB-Core U1461B 86X clearly show that gravy is characterized by higher bulk density compared to biscuits (Fig. 4).

3.2 Micro-computed tomography (CT) scans

Micro-computed tomography (μ CT) images were captured of small cubes of sediment from three adjacent sections from Hole U1463B, spanning the switch in coring technique from HLAPC to XCB. Samples come from sections U1463B 33F2 and 33F3 (281.20–284.16 m CSF-A) and section U1463B 34X1 (284.40–285.90 m CSF-A), all belonging to the same lithostratigraphic subunit. The samples were deliberately chosen to be closely spaced stratigraphically on ei-

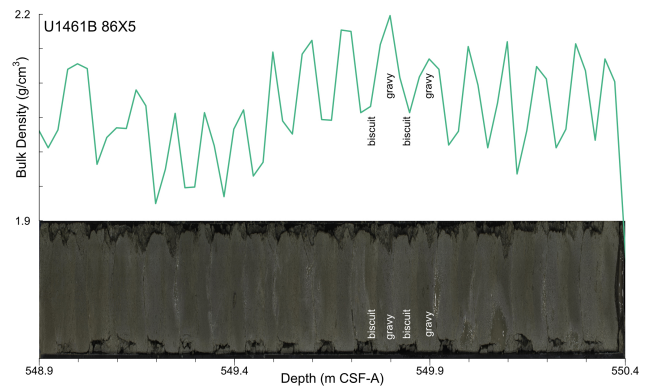


Figure 4. The effect of the biscuit-and-gravy core disturbance on bulk density in XCB cores. Gravy is characterized by a higher bulk density compared to biscuits.

ther side of the HLAPC-XCB switch. This sampling allows for an assessment of the impact of drilling technique while at the same time limiting stratigraphic variability along the depth axis. The only core disturbance recorded by the ship-board sedimentologists in this interval is moderate gravy and biscuits in section U1463B 34X1. However, we note that core pictures of section U1463 33F3 reveal a slight deformation of the sediment, with uparching bed contacts and indications of vertical flowage of sediment along the core liner (Jutzeler et al., 2014).

The smallest micro-pores, which measure $< 0.002 \text{ mm}^3$, appear as dark purple volumes in the images, while foraminifera are shown in yellow, typically measuring $0.003\text{--}0.005 \text{ mm}^3$ (Fig. 5a–f). The comparison of μ CT images according to drilling technique seems to suggest that XCB samples are characterized by a greater abundance of micro-pores in comparison to APC cores. The quantification of Feret diameters of identified pores in the CT images supports this visual observation. The distribution of Feret diameters is more right-skewed, with a higher mode for pores with a $\sim 0.1 \text{ mm}$ diameter. The XCB cores thus appear to exhibit a higher abundance of micro-pores ($< 0.002 \text{ mm}^3$) compared to the APC cores.

3.3 SEM imaging of pore space and cements

SEM analysis allowed the state of pore space and cements to be observed in great detail (Fig. 6a, b). The XCB-derived samples exhibit calcite cements well attached to primary sediment grains (Fig. 6c) and build a cemented structure within the sediment, indicative of early lithification. The HLAPC-derived samples, on the other hand, also contain calcite cement crystals (Fig. 6b, d), though the cements are unattached to sediment grains, and the pore volume seems reduced (Fig. 6d). This detachment can also be observed for sediment grains such as foraminifera, which are separated by a thin gap from the formerly attached matrix (Fig. 6f).

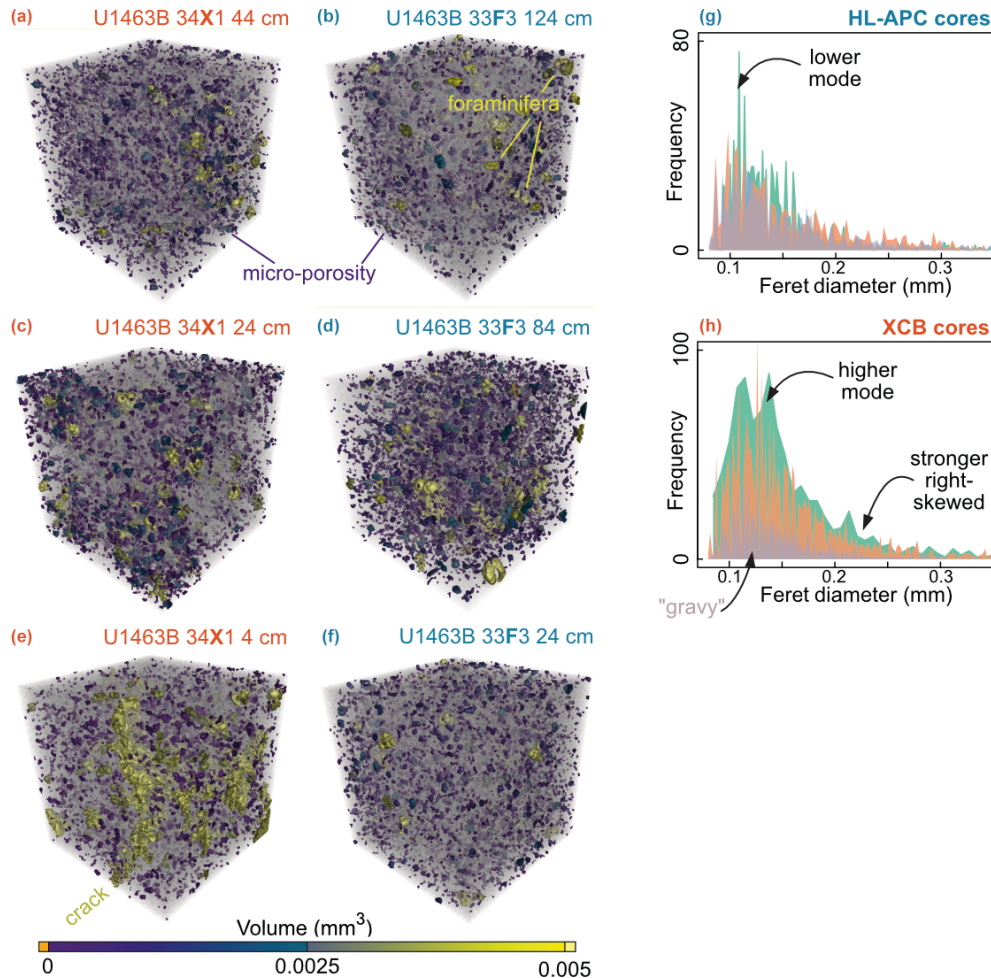


Figure 5. Micro-porosity as captured by μ CT images of adjacent HL-APC and XCB cores at Hole U1463B. (a–f) XCB samples exhibit slightly more abundant and slightly larger micro-pores ($< 0.002 \text{ mm}^3$, purple) than APC cores. However, we acknowledge that the difference is hard to discern visually. Foraminifera and cracks within the samples are depicted in yellow. (g–h) The distribution of Feret diameters helps to visualize the difference in micro-porosity, with a more right-skewed distribution and a higher mode for XCB cores compared to HL-APC samples. Note that the samples are all from the same hole, closely spaced ($\pm 1 \text{ m}$) on either side of the HL-APC-XCB switch in Hole U1463B.

4 Discussion

The data presented from Sites U1463 and U1464 indicate that the (HL)APC technique utilized by IODP potentially leads to the partial loss of lithification and a reduction in P-wave velocity. Additionally, micro-porosity in APC cores seems lower than equivalent XCB cores, resulting in noticeable effects on bulk density and porosity. We suspect that the hydraulic force exerted by the inner core barrel of an APC core as it penetrates the sediment is the most probable explanation for this observation.

The APC coring technique is known to produce high-quality and high-resolution sedimentary records for paleoclimate purposes, preserving original sedimentary structures as well as soft-sediment deformations. However, the pressure wave that is sent through the sedimentary formation exerts a dynamic stress on the individual grains. The piston force of

(HL-)APC coring can amount up to 125 kN (JOIDES Resolution Science Operator, 2014). This stress can lead to a temporary rearrangement of the grains. Essentially, the wave creates a temporary increase in pressure that pushes the grains closer together, resulting in a more tightly packed arrangement, i.e. condensation. The effect is often referred to as “acoustic compaction” and could explain the changes in the physical properties of the sediment, such as increased density and reduced porosity (Figs. 2, 3) and fewer micro-pores (Fig. 5). Here, we illustrate this effect by means of SEM images, showing a much denser packing of carbonate grains and clay minerals in the APC core (Fig. 6b) compared to the adjacent XCB core (Fig. 6a).

Another potential effect of the APC-generated pressure wave is the breaking of early cements in a carbonate sediment. The XCB-core SEM images in Fig. 6c exhibit continuous, uninterrupted sparitic cements, connecting different

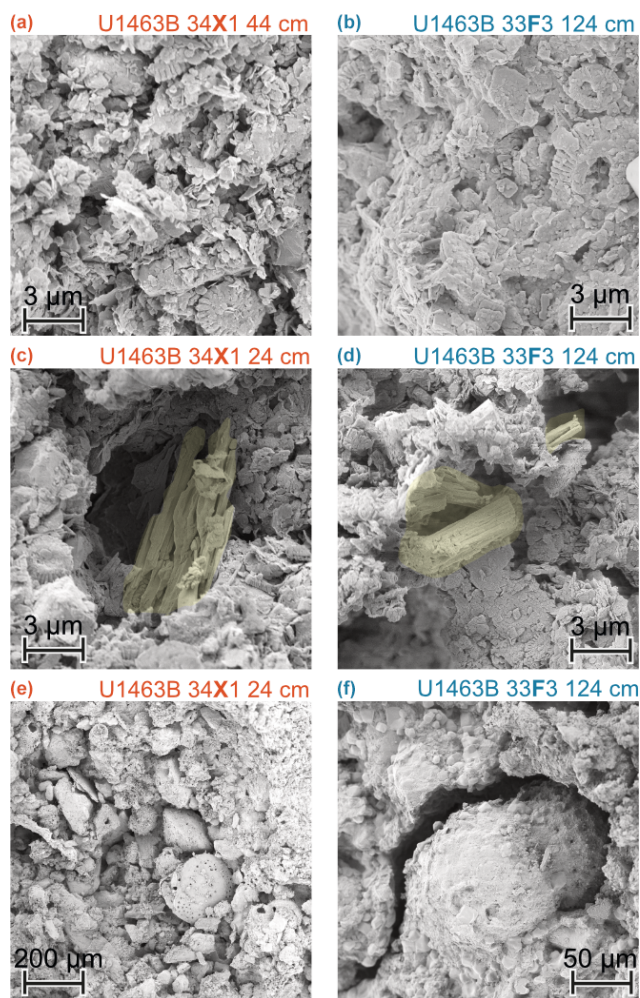


Figure 6. Scanning electron microscope (SEM) pictures of adjacent HLAPC and XCB cores at Hole U1463B. **(a)** Loosely packed matrix consisting of clay minerals and nanofossils, allowing for a high abundance of micro-pores. **(b)** Densely packed matrix consisting of clay minerals and nanofossils. **(c)** Sparitic cement (highlighted in yellow) growing in a loosely packed matrix of clay minerals and nanofossils. **(d)** Disaggregated, broken sparitic crystal (highlighted in yellow) in a matrix of clay minerals and nanofossils. **(e)** Overview image showing a benthic foraminifer in a loosely packed matrix. **(f)** Planktic foraminifer that is fully separated from its densely packed matrix by a micro-crack. Note that the samples are all from the same hole, closely spaced (± 1 m) on either side of the HLAPC-XCB switch in Hole U1463B.

components of the carbonate mudstone and often overgrowing the clay matrix. However, similar sparitic cements appear broken and disrupted in Fig. 6d, which is from an adjacent APC core. These images suggest that the APC-generated pressure wave may have caused the cements to break apart and become discontinuous. This effect likely constitutes the underlying reason for the observed differences in lithification of the sediment between XCB and APC cores. Moreover, the disruption of early cements could also explain the

large offset in P-wave velocity measured between the APC and XCB cores. A P-wave travels through the sedimentary formation faster when it can use early cements as a pathway between different components of the sediment. However, when these cements are discontinued, as in the case of the APC cores (Fig. 6d), the P-wave needs to travel around, leading to a lower velocity. It seems likely that the APC-core sediments and XCB-core gravity exhibit similar P-wave velocities because both lack the connectivity of early cements. For the first, inter-grain early cements, as well as possibly inter-grain pressure-solution bindings, are destroyed by the APC-generated pressure wave, whereas for the latter, the sediment grinding by rotary drilling is responsible for the loss of sedimentary strength and gravity production.

In addition to the breaking of early cements, another factor that might have contributed to the lower P-wave velocities in APC cores is the detaching of components like foraminifera and other bioclasts from the surrounding matrix. For instance, the SEM image in Fig. 6f illustrates a planktonic foraminifer that appears disconnected from its densely packed micritic matrix. We suspect that this detachment could have been the result of the hydraulic pressure wave travelling through the sediment upon APC coring. In contrast, we juxtapose this image with an image of a benthic foraminifer in an XCB core that occurs in a loosely packed matrix (Fig. 6e). The detachment and possible fracturing of carbonate components might have contributed to a reduction in inter-grain contacts and, as a consequence, a lower P-wave velocity in APC cores.

The impact of coring technique on the physical appearance of carbonate sediments poses a challenge to sedimentologists studying early diagenesis and lithification. APC coring destroys early cements and causes an artificially increased packing of sedimentary grains. Conversely, XCB cores destroy large parts of the original sedimentary fabrics and textures by producing gravity, leaving only biscuits as snapshots of the original sedimentary formation. The results of this study thus highlight the necessity to keep developing new scientific drilling techniques that are better aligned with the scientific needs of sedimentological research towards lithification and early diagenesis. The extended nose sampler could be such an option, whereby the core barrel is not fired into the formation. Instead, the core barrel is pushed into the formation, increasing the push force when hard formations are encountered, and vice versa.

5 Conclusions

The results of this study demonstrate that there are significant differences between the lithology and physical properties of sediments recovered by APC and XCB techniques in carbonate sediments. While APC coring remains the gold standard for paleoceanography research due to its ability to provide continuous, high-quality cores over long intervals, the data

presented here suggest that XCB cores may give a more accurate representation of the micro-porosity, inter-grain connections, and P-wave velocity of the cored sedimentary formation. Indeed, the hydraulic pressure wave generated during the deployment of the APC-core barrel can cause acoustic compaction and can cause early sparitic cements to disaggregate, thereby destroying early lithification and the accompanying sedimentary features.

For that reason, we make researchers interested in studying early diagenetic pathways in carbonate sediments from IODP cores aware of this phenomenon and recommend the use of XCB biscuits cores instead of APC cores in overlapping intervals in carbonate sediments. Indeed, XCB biscuits may provide more valuable insights into the microstructure and lithification of the sedimentary formation in such cases. Ideally, a combination of APC and XCB coring should be applied to provide a complete picture of lithification and sediment composition when studying early diagenetic pathways. To do so, it would be interesting to also experiment with alternative coring tools, like the extended nose corer (JOIDES Resolution Science Operator, 2014; Talalay, 2022). This coring tool potentially offers an intermediate solution between APC and XCB, whereby a core liner is pushed into the sediment without the immense hydraulic pressure. To date, it also remains unclear as to what extent this issue extends into other, more cohesive lithologies. Nevertheless, this study highlights the importance of carefully considering the choice of coring technique when planning sediment coring programmes and when interpreting subsequent analyses.

Data availability. The physical property data, core pictures, and downhole logging data presented in Figs. 2 and 3 are available from the IODP LIMS database (<https://web.iodp.tamu.edu/LORE/>, JOIDES Resolution Science Operator, 2023) and the IODP logging database (<https://mlp.ldeo.columbia.edu/logdb/>, Columbia University, 2023). Raw data of micro-CT scans and SEM images are available from De Vleeschouwer et al. (2023).

Author contributions. DDV, TN, and GA conceptualized the research. GA carried out the SEM images. CS carried out the micro-CT analyses. All authors contributed to the interpretation of the results. DDV wrote the paper with input of all co-authors.

Competing interests. The contact author has declared that none of the authors has any competing interests.

Disclaimer. Publisher's note: Copernicus Publications remains neutral with regard to jurisdictional claims in published maps and institutional affiliations.

Acknowledgements. This research used samples and data provided by the International Ocean Discovery Program (IODP). We thank all IODP Expedition 356 scientific participants and crew for making this study possible. Special thanks go to Michelle Kominz (Western Michigan University) for pointing out the remarkable difference in lithification during the expedition. We are also grateful to the European Consortium for Ocean Research and Drilling (ECORD) for funding the MagellanPlus Workshop “TIMOR – Tracing Monsoon, Ocean currents and diagenetic carbon redistribution) on 19–22 May 2022 in Vienna, Austria. We thank Christian Vollmer (University of Münster) for technical assistance. We thank David McInroy and Robert McKay for their constructive and thoughtful reviews.

Review statement. This paper was edited by Ulrich Harms and reviewed by David McInroy and Robert McKay.

References

- Bathurst, R. G. C.: Carbonate sediments and their diagenesis, Developments in sedimentology, Elsevier, 658 pp., ISBN 978-0-444-40891-4, 1972.
- Bathurst, R. G. C.: Marine diagenesis of shallow water calcium carbonate sediments, *Annu. Rev. Earth Pl. Sci.*, 2, 257–274, 1974.
- Bathurst, R. G. C.: Lithification of carbonate sediments, *Sci. Prog.*, 66, 451–471, 1980.
- Berner, R. A.: Early diagenesis: A theoretical approach, 1, Princeton University Press, ISBN 9780691082608, 256 pp., 1980.
- Blum, P.: Physical properties handbook: A guide to the shipboard measurement of physical properties of deep-sea cores, ODP Tech. Note, 26, 113 pp., <https://doi.org/10.2973/odp.tn.26.1997>, 1997.
- Budd, D. A.: Cenozoic dolomites of carbonate islands: Their attributes and origin, *Earth-Sci. Rev.*, 42, 1–47, [https://doi.org/10.1016/S0012-8252\(96\)00051-7](https://doi.org/10.1016/S0012-8252(96)00051-7), 1997.
- Buryakovskiy, L., Chilingar, G. V., Rieke, H. H., and Shin, S.: Fundamentals of the petrophysics of oil and gas reservoirs, John Wiley & Sons, ISBN 978-1-118-34447-7, 400 pp., 2012.
- Christensen, B. A., Renema, W., Henderiks, J., De Vleeschouwer, D., Groeneveld, J., Castañeda, I. S., Reuning, L., Bogus, K., Auer, G., Ishiwa, T., McHugh, C. M., Gallagher, S. J., Fulthorpe, C. S., and Scientists, I. E.: Indonesian throughflow drove austral climate from humid pliocene to arid pleistocene, *Geophys. Res. Lett.*, 44, 6914–6925, <https://doi.org/10.1002/2017GL072977>, 2017.
- De Vleeschouwer, D., Nohl, T., Schulbert, C., Bialik, O. M., and Auer, G.: Coring tools have an effect on lithification and physical properties of marine carbonate sediments, Zenodo [data set], <https://doi.org/10.5281/zenodo.8319206>, 2023.
- Columbia University: Division of Marine and Large Programs, Search Logging Data, Columbia University [data set], <https://mlp.ldeo.columbia.edu/logdb/> (last access: 10 September 2023), 2023.
- Fabricius, I. L.: How burial diagenesis of chalk sediments controls sonic velocity and porosity, *AAPG Bull.*, 87, 1755–1778, <https://doi.org/10.1306/06230301113>, 2003.

- Flügel, E.: *Microfacies analysis of limestones*, Springer Berlin, Heidelberg, 634 pp., <https://doi.org/10.1007/978-3-642-68423-4>, 1982.
- Folk, R. L., Pray, L. C., and Murray, R. C.: Some aspects of recrystallization in ancient limestones, in: *Dolomitization and limestone diagenesis*, SEPM Society for Sedimentary Geology, 13, 14–48, <https://doi.org/10.2110/pec.65.07.0014>, 1965.
- Friedman, G. M.: Early diagenesis and lithification in carbonate sediments, *J. Sediment Res.*, 34, 777–813, <https://doi.org/10.1306/74d71195-2b21-11d7-8648000102c1865d>, 1964.
- Froelich, P. N., Klinkhammer, G. P., Bender, M. L., Luedtke, N. A., Heath, G. R., Cullen, D., Dauphin, P., Hammond, D., Hartman, B., and Maynard, V.: Early oxidation of organic matter in pelagic sediments of the eastern equatorial atlantic: Suboxic diagenesis, *Geochim. Cosmochim. Ac.*, 43, 1075–1090, [https://doi.org/10.1016/0016-7037\(79\)90095-4](https://doi.org/10.1016/0016-7037(79)90095-4), 1979.
- Gallagher, S., Fulthorpe, C., Bogus, K., Auer, G., Baranwal, S., Castañeda, I., Christensen, B., Vleeschouwer, D. D., Franco, D., and Groeneveld, J.: Expedition 356 summary, 43 pp., <https://doi.org/10.14379/iodp.proc.356.101.2017>, 2017a.
- Gallagher, S. J., Fulthorpe, C. S., Bogus, K., Auer, G., Baranwal, S., Castañeda, I. S., Christensen, B. A., De Vleeschouwer, D., Franco, D. R., Groeneveld, J., Gurnis, M., Haller, C., He, Y., Henderiks, J., Himmler, T., Ishiwa, T., Iwatani, H., Jatinigrum, R. S., Kominz, M. A., Korpanty, C. A., Lee, E. Y., Levin, E., Mamo, B. L., McGregor, H. V., McHugh, C. M., Petrick, B. F., Potts, D. C., Rastegar Lari, A., Renema, W., Reuning, L., Takayanagi, H., and Zhang, W.: Expedition 356 methods, in: *Indonesian throughflow*, edited by: Gallagher, S. J., Fulthorpe, C. S., Bogus, K., and the Expedition 356 Scientists, Proceedings of the International Ocean Discovery Program, College Station, TX, <https://doi.org/10.14379/iodp.proc.356.102.2017>, 2017b.
- Gallagher, S. J., Fulthorpe, C. S., Bogus, K., Auer, G., Baranwal, S., Castañeda, I. S., Christensen, B. A., De Vleeschouwer, D., Franco, D. R., Groeneveld, J., Gurnis, M., Haller, C., He, Y., Henderiks, J., Himmler, T., Ishiwa, T., Iwatani, H., Jatinigrum, R. S., Kominz, M. A., Korpanty, C. A., Lee, E. Y., Levin, E., Mamo, B. L., McGregor, H. V., McHugh, C. M., Petrick, B. F., Potts, D. C., Rastegar Lari, A., Renema, W., Reuning, L., Takayanagi, H., and Zhang, W.: Site u1463, in: *Indonesian throughflow*, edited by: Gallagher, S. J., Fulthorpe, C. S., Bogus, K., and the Expedition 356 Scientists, Proceedings of the International Ocean Discovery Program, College Station, TX, <https://doi.org/10.14379/iodp.proc.356.108.2017>, 2017c.
- Garrison, R. E. and Kennedy, W. J.: Origin of solution seams and flaser structure in upper cretaceous chalks of southern england, *Sediment Geol.*, 19, 107–137, [https://doi.org/10.1016/0037-0738\(77\)90027-6](https://doi.org/10.1016/0037-0738(77)90027-6), 1977.
- Ge, Y., Pederson, C. L., Lokier, S. W., Traas, J. P., Nehrke, G., Neuser, R. D., Goetschl, K. E., and Immenhauser, A.: Late holocene to recent aragonite-cemented transgressive lag deposits in the abu dhabi lagoon and intertidal sabkha, *Sedimentology*, 67, 2426–2454, <https://doi.org/10.1111/sed.12707>, 2020.
- Harris, P. M., Kendall, C. G. S. C., Lerche, I., Schneidermann, N., and Harris, P. M.: Carbonate cementation – a brief review, in: *Carbonate cements: Based on a symposium sponsored by the society of economic paleontologists and mineralogists*, SEPM Society for Sedimentary Geology, 36, 79–96, <https://doi.org/10.2110/pec.85.36.0079>, 1985.
- Hendy, A. J.: Taphonomic overprints on phanerozoic trends in biodiversity: Lithification and other secular megabiases, in: *Taphonomy. Aims & scope topics in geobiology book series*, edited by: Allison, P. A. and Bottjer, D. J., Springer, Dordrecht, 19–77, https://doi.org/10.1007/978-90-481-8643-3_2, 2011.
- Herbert, T. D.: Differential compaction in lithified deep-sea sediments is not evidence for “diagenetic unmixing”, *Sediment Geol.*, 84, 115–122, [https://doi.org/10.1016/0037-0738\(93\)90049-B](https://doi.org/10.1016/0037-0738(93)90049-B), 1993.
- JOIDES Resolution Science Operator: Coring tools and technology: <https://iodp.tamu.edu/tools/index.html> (last access: 8 August 2023), 2014.
- JOIDES Resolution Science Operator: IODP LIMS database, <https://web.iodp.tamu.edu/LORE/> (last access: 10 September 2023), 2023.
- Jutzeler, M., White, J. D. L., Talling, P. J., McCanta, M., Morgan, S., Le Friant, A., and Ishizuka, O.: Coring disturbances in iodp piston cores with implications for offshore record of volcanic events and the missoula megafloods, *Geochem. Geophys. Geos.*, 15, 3572–3590, <https://doi.org/10.1002/2014GC005447>, 2014.
- Mavromatis, V., Meister, P., and Oelkers, E. H.: Using stable mg isotopes to distinguish dolomite formation mechanisms: A case study from the peru margin, *Chem. Geol.*, 385, 84–91, <https://doi.org/10.1016/j.chemgeo.2014.07.019>, 2014.
- MCKenzie, J. A. and Vasconcelos, C.: Dolomite mountains and the origin of the dolomite rock of which they mainly consist: Historical developments and new perspectives, *Sedimentology*, 56, 205–219, <https://doi.org/10.1111/j.1365-3091.2008.01027.x>, 2009.
- Moore, C. H. and Wade, W. J.: Chapter 5 – carbonate diagenesis: Introduction and tools, in: *Developments in sedimentology*, edited by: Moore, C. H., and Wade, W. J., Elsevier, 67–89, <https://doi.org/10.1016/B978-0-444-53831-4.00005-7>, 2013.
- Munnecke, A.: Bildung mikritischer kalke im silur auf gotland, *Cour Forsch Senck*, 198, 1–131, 1997.
- Munnecke, A. and Samtleben, C.: The formation of micritic limestones and the development of limestone-marl alternations in the silurian of gotland, sweden, *Facies*, 34, 159–176, <https://doi.org/10.1007/BF02546162>, 1996.
- Munnecke, A., Wright, V. P., and Nohl, T.: The origins and transformation of carbonate mud during early marine burial diagenesis and the fate of aragonite: A stratigraphic sedimentological perspective, *Earth-Sci. Rev.*, 239, 104366, <https://doi.org/10.1016/j.earscirev.2023.104366>, 2023.
- Nawrot, R.: Decomposing lithification bias: Preservation of local diversity structure in recently cemented storm-beach carbonate sands, san salvador island, bahamas, *Palaios*, 27, 190–205, <https://doi.org/10.2110/palo.2011.p11-028r>, 2012.
- Nohl, T., Jarochowska, E., and Munnecke, A.: Revealing the genesis of limestone-marl alternations: A taphonomic approach, *Palaios*, 34, 15–31, <https://doi.org/10.2110/palo.2018.062>, 2019.
- Nohl, T., Steinbauer, M. J., Sinnesael, M., and Jarochowska, E.: Detecting initial aragonite and calcite variations in limestone-marl alternations, *Sedimentology*, 68, 3102–3115, <https://doi.org/10.1111/sed.12885>, 2021.
- Reid, R. P., Visscher, P. T., Decho, A. W., Stolz, J. F., Bebout, B. M., Dupraz, C., Macintyre, I. G., Paerl, H. W., Pinckney, J. L., Prufert-Bebout, L., Stepe, T. F., and DesMarais, D. J.:

- The role of microbes in accretion, lamination and early lithification of modern marine stromatolites, *Nature*, 406, 989–992, <https://doi.org/10.1038/35023158>, 2000.
- Reuning, L., Deik, H., Petrick, B., Auer, G., Takayanagi, H., Iryu, Y., Courtillot, M., and Bassetti, M.-A.: Contrasting intensity of aragonite dissolution and dolomite cementation in glacial versus interglacial intervals of a subtropical carbonate succession, *Sedimentology*, 69, 2131–2150, <https://doi.org/10.1111/sed.12985>, 2022.
- Rosenthal, Y., Holbourn, A. E., Kulhanek, D. K., Aiello, I. W., Babila, T. L., Bayon, G., Beaufort, L., Bova, S. C., Chun, J.-H., Dang, H., Drury, A. J., Dunkley Jones, T., Eichler, P. P. B., Fernando, A. G. S., Gibson, K. A., Hatfield, R. G., Johnson, D. L., Kumagai, Y., Li, T., Linsley, B. K., Meinicke, N., Mountain, G. S., Opdyke, B. N., Pearson, P. N., Poole, C. R., Ravelo, A. C., Sagawa, T., Schmitt, A., Wurtzel, J. B., Xu, J., Yamamoto, M., and Zhang, Y. G.: U1482, in: *Western pacific warm pool*, edited by: Rosenthal, Y., Holbourn, A. E., Kulhanek, D. K., and the Expedition 363 Scientists, International Ocean Discovery Program, College Station, TX, <https://doi.org/10.14379/iodp.proc.363.103.2018>, 2018.
- Ryan, G., Bernardel, G., Kennard, J., Jones, A. T., Logan, G., and Rollet, N.: A pre-cursor extensive miocene reef system to the rowley shoals reefs, western australia: Evidence for structural control of reef growth or natural hydrocarbon seepage?, *The APPEA Journal*, 49, 337–364, <https://doi.org/10.1071/AJ08021>, 2009.
- Sample, J. C., Torres, M. E., Fisher, A., Hong, W.-L., Destigneville, C., Defliese, W. F., and Tripathi, A. E.: Geochemical constraints on the temperature and timing of carbonate formation and lithification in the nankai trough, nantroseize transect, *Geochim. Cosmochim. Ac.*, 198, 92–114, <https://doi.org/10.1016/j.gca.2016.10.013>, 2017.
- Shinn, E. A.: Submarine lithification of holocene carbonate sediments in the persian gulf, *Sedimentology*, 12, 109–144, <https://doi.org/10.1111/j.1365-3091.1969.tb00166.x>, 1969.
- Sinnesael, M., De Vleeschouwer, D., Zeeden, C., Batenburg, S. J., Da Silva, A.-C., de Winter, N. J., Dinarès-Turell, J., Drury, A. J., Gambacorta, G., Hilgen, F. J., Hinnov, L. A., Hudson, A. J. L., Kemp, D. B., Lantink, M. L., Laurin, J., Li, M., Liebrand, D., Ma, C., Meyers, S. R., Monkenbusch, J., Montanari, A., Nohl, T., Pälke, H., Pas, D., Ruhl, M., Thibault, N., Vahlenkamp, M., Valero, L., Wouters, S., Wu, H., and Claeys, P.: The cyclostratigraphy intercomparison project (cip): Consistency, merits and pitfalls, *Earth-Sci. Rev.*, 199, 102965, <https://doi.org/10.1016/j.earscirev.2019.102965>, 2019.
- Soetaert, K., Hofmann, A. F., Middelburg, J. J., Meysman, F. J. R., and Greenwood, J.: Reprint of “the effect of biogeochemical processes on ph”, *Mar. Chem.*, 106, 380–401, <https://doi.org/10.1016/j.marchem.2007.06.008>, 2007.
- Sulpis, O., Agrawal, P., Wolthers, M., Munhoven, G., Walker, M., and Middelburg, J. J.: Aragonite dissolution protects calcite at the seafloor, *Nat. Commun.*, 13, 1104, <https://doi.org/10.1038/s41467-022-28711-z>, 2022.
- Tagliavento, M., John, C. M., Anderskouv, K., and Stemmerik, L.: Towards a new understanding of the genesis of chalk: Diagenetic origin of micarbs confirmed by clumped isotope analysis, *Sedimentology*, 68, 513–530, <https://doi.org/10.1111/sed.12802>, 2021.
- Talalay, P. G.: Geological and scientific offshore drilling and core sampling in ice-covered waters, in: *Geotechnical and exploration drilling in the polar regions*, edited by: Talalay, P. G., Springer International Publishing, Cham, 339–383, https://doi.org/10.1007/978-3-031-07269-7_11, 2022.
- Wurgaft, E., Findlay, A. J., Vigderovich, H., Herut, B., and Sivan, O.: Sulfate reduction rates in the sediments of the mediterranean continental shelf inferred from combined dissolved inorganic carbon and total alkalinity profiles, *Mar. Chem.*, 211, 64–74, <https://doi.org/10.1016/j.marchem.2019.03.004>, 2019.